energies

MDPI

Article

Enhancing CO_2 Hydrogenation to Methane by Ni-Based Catalyst with V Species Using 3D-mesoporous KIT-6 as Support

Hongxia Cao [1,2,3,4,*], Wenyuan Wang [3], Tianlei Cui [3], Hongyan Wang [1,3], Guang Zhu [1] and Xiangkun Ren [4]

1 Key Laboratory of Spin Electron and Nanomaterials of Anhui Higher Education Institutes, Suzhou University, Suzhou 234000, China; suzhouwhy@163.com (H.W.); guangzhu@ahszu.edu.cn (G.Z.)
2 Jiangsu Province Engineering Laboratory of High Efficient Energy Storage Technology and Equipments, China University of Mining and Technology, Xuzhou 221116, China
3 School of Chemistry and Chemical Engineering, Suzhou University, Suzhou 234000, China; wyc6@foxmail.com (W.W.); cuitianlei163@163.com (T.C.)
4 Low Carbon Energy Institute, China University of Mining and Technology, Xuzhou 221008, China; xiangkunren@cumt.edu.cn
* Correspondence: hxcao@ahszu.edu.cn; Tel.: +86-1875-211-8972

Received: 12 March 2020; Accepted: 29 April 2020; Published: 3 May 2020

Abstract: Using renewable H_2 for CO_2 hydrogenation to methane not only achieves CO_2 utilization, but also mitigates the greenhouse effect. In this work, several Ni-based catalysts with V species using 3D-mesoporous KIT-6 (Korea Advanced Institute of Science and Technology, KIT) as support were prepared at different contents of NiO and V_2O_5. Small Ni nanoparticles with high dispersibility on 20Ni-0.5V/KIT-6 were identified by X-ray diffraction (XRD), TEM and hydrogen temperature-programmed desorption (H_2-TPD) analysis, which promoted the production of more Ni active sites for enhancing catalytic activity for CO_2 methanation. Moreover, TEM and hydrogen temperature-programmed reduction (H_2-TPR) characterizations confirmed that a proper amount of Ni and V species was favorable to preserve the 3D-mesoporous structure and strengthen the interaction between active Ni and KIT-6. The synergistic effect between Ni and V could strengthen surface basicity to elevate the ability of CO_2 activity on the 20Ni-0.5V/KIT-6. In addition, a strong interaction with the 3D-mesoporous structure allowed active Ni to be firmly anchored onto the catalyst surface, which was accountable for improving catalytic activity and stability. These results revealed that 20Ni-0.5V/KIT-6 was a catalyst with superior catalytic activity and stability, which was considered as a promising candidate for CO_2 hydrogenation to methane.

Keywords: CO_2 methanation; Ni-based catalyst; KIT-6; 3D-mesoporous; V species

1. Introduction

In the recent decades, the amount of CO_2 in the atmosphere rose rapidly due to the ongoing consumption of carbon-based fuels, including coal, petroleum and natural gas, which are regarded as the leading reasons for the greenhouse effect [1–4]. To alleviate CO_2 emissions, numerous efforts have been devoted to developing effective CO_2 capture, storage, and utilization technologies [5–8]. Among these schemes, the reaction of CO_2 with renewable H_2 to produce synthetic natural gas, also named as CO_2 methanation [9,10], is considered as a promising approach for CO_2 reduction because the generated CH_4 can be readily stored in the existing gas grid or utilized as raw materials in the chemical industry [11,12].

$$CO_2 + 4H_2 \rightarrow CH_4 + 2H_2O(\Delta H^o = -165\ KJ/mol) \quad (1)$$

As illustrated in Equation (1), CO_2 methanation is an exothermic reaction. Correspondingly, for yielding a higher equilibrium concentration of CH_4, CO_2 methanation should be performed at a low temperature. Unfortunately, it is extremely difficult to activate CO_2 due to the large activation barrier for CO_2 reduction [13,14]. Therefore, effective catalysts are in urgent need for CO_2 methanation to attain superior catalytic activity and stability.

Usually, precious metals, such as Ru [15–17], Rh [18,19] and Pd [20], are considered as the ideal candidates to prepare catalysts for CO_2 methanation because of their excellent catalytic performance. Nevertheless, they are not widely applied in industry owing to their relatively high cost. In comparison with the catalysts containing precious metals, Ni-based catalysts with comparable catalytic activity and relatively low costs have been extensively investigated for CO_2 methanation [21–25]. However, Ni-based catalysts are apt to deactivate even under low temperature because of the aggregation of Ni nanoparticles and carbon deposition [26].

In recent years, using a mesoporous Si molecular sieve as support is regarded as an effective way to enhance Ni dispersion, anti-sintering and carbon-resistance, because they possess a large specific surface area, adjustable pore size and high hydrothermal stability [27]. Bacariza et al. [28] fabricated an Ni-based MCM-41 catalyst, which presented high CO_2 conversion. Moreover, as reported by Lu et al. [29], the Ni-grafted SBA-15 catalyst was suitable for CO_2 methanation because its cage-type mesoporous structure facilitated the formation of small Ni nanoparticles, resulting in an improvement in the catalytic performance [30]. Although partial progress has been made, it is still hard to suppress the coke formation and sintering of Ni nanoparticles while achieving a high catalytic activity. Recently, it has been reported that V species as a promoter can reduce the energy barrier of CO_2 methanation to promote CO_2 activation on the catalyst, subsequently enhancing the catalytic activity at low temperatures [31]. Furthermore, the addition of V species are able to facilitate Ni dispersion and accelerate CO dissociation, enhancing catalytic CO_2 methanation. Li et al. [32] revealed that, in V-containing catalysts, an intimate contact between active Ni and the support greatly influenced the dispersion of active phase on the support. Based on these promising results, it was concluded that catalytic CO_2 methanation can be significantly enhanced by the improvement of the catalytic structure and Ni dispersion using a mesoporous Si molecular sieve as support and adding V species as promoter.

This work focused on the development of a series of Ni-based catalysts with V species using 3D-mesoporous KIT-6 as support for enhancing catalytic CO_2 methanation. As one of the mesoporous Si molecular sieves, 3D-mesoporous KIT-6, with a larger specific surface area and pore volume, is composed of two interwoven subnetworks [33] which are favorable to the formation of highly dispersed nanoparticles for enhancing catalytic performance. Moreover, the effects of NiO and V_2O_5 loading on catalytic CO_2 methanation were explored, as well as X-ray diffraction (XRD), hydrogen temperature-programmed reduction (H_2-TPR), hydrogen temperature-programmed desorption (H_2-TPD), carbon dioxide temperature-programmed desorption (CO_2-TPD), thermogravimetric analysis (TGA), transmission electron microscope (TEM), and energy-dispersive X-ray spectroscopy (EDX) were employed to characterize the catalysts. Furthermore, a 60h-lifetime test was performed to investigate the catalytic stability.

2. Materials and Methods

2.1. Catalyst Preparation

KIT-6 with 3D mesopores was fabricated according to the experimental scheme reported by Kleitz et al. [34]. Typically, 4 g P123 was added into the hydrochloric acid solution composing of 144 mL H_2O and 6 ml HCl (35%) at 35 °C, accompanied by a subsequent addition of 1-butanol (4.9 mL) and TEOS (9.2 mL) as the silicon source. The resulting slurry was hydrothermally treated in a Teflon bottle at 100 °C for 24 h. The solid product collected by filtration and washing was dried at 100 °C for 24 h, followed by a 550 °C calcination in air for 4 h to obtain a white power with a synthesis yield of

around 92%, denoted as KIT-6. As a support, KIT-6 modified by ethylene glycol was impregnated into a Ni aqueous solution with 10 wt.% NiO. After evaporation at 60 °C for 10 h, the solid product was dried and calcined at 550 °C for 4 h to acquire a KIT-6 supported Ni-based catalyst, named as 10Ni/KIT-6. Moreover, 10Ni-0.5V/KIT-6 was synthesized by employing a similar procedure as that used in the literature [35]. KIT-6 modified by ethylene glycol was dispersed in an aqueous solution containing 10 wt.% NiO and 0.5 wt.% V_2O_5 and then kept stirring at 60 °C for 10 h. After drying at 100 °C and calcination at 550 °C, the final product with a synthesis yield of around 95% was named as 10Ni-0.5V/KIT-6. In addition, 10Ni-*y*V/KIT-6 (y = 0.1, 0.5, 1, 2) was prepared with 10 wt.% NiO and different contents of V_2O_5 (0.1 wt.%, 0.5 wt.%, 1 wt.%, 2 wt.%). Similarly, xNi-0.5V/KIT-6 (x = 5, 10, 20, 40) was synthesized with 0.5 wt.% V_2O_5 and various contents of NiO (5 wt.%, 10 wt.%, 20 wt.%, 40 wt.%).

2.2. Catalyst Characterization

Wide-angle XRD pattern from 10° to 80° was obtained at a scanning speed of 8°/min using a diffractometer with Cu Kα radiation (D/MAX 2500, Rigaku, Tokyo, Japan) and low-angle XRD measurement was achieved at 1°/min from 0.5° to 5°. Ni crystallite size was estimated using the Debye–Scherrer equation. TEM images with EDX were characterized to explore the morphology and elemental distribution based on an equipment with a 200 kV acceleration voltage (Tecnai G2 F20, FEI, Hillsboro, OR, USA). The carbon content deposited on spent catalyst was assessed by a thermogravimetric analyzer (STA449F3, Netzsch, Selb, Germany) with a temperature ramp of 10 °C/min in air. H_2-TPR profiles ranging from room temperature to 800 °C were recorded using an instrument in 10 vol.% H_2/Ar with a heating rate of 10 °C/min (Auto Chem 2910, Micromeritics, Norcross, GA, USA). H_2-TPD was measured on the same instrument as H_2-TPR. Prior to experiment, each sample was heated to 550 °C and kept for 2 h in 30 mL/min H_2 for reducing Ni^{2+} to Ni^0. When the temperature dropped to 50 °C, Ar flow was introduced to purge the physically adsorbed H_2. H_2-TPD curves were obtained according to the amount of desorbed H_2 in Ar flow by heating sample to 800 °C at a ramping rate of 10 °C/min. Ni dispersion was calculated by referencing to the previous publication [36]. CO_2-TPD was investigated following the same procedure as H_2-TPD in addition to using CO_2 instead of H_2 in the adsorption and desorption steps.

2.3. Catalytic Performance Measurement

Catalytic activity test for CO_2 methanation was conducted at atmospheric pressure and at different reaction temperatures in a continuous flow fixed-bed reactor. An amount of 50 mg catalyst, diluted with 500 mg quartz sand, was placed in the center of the quartz tube. The real-time reaction temperature of the catalyst bed center was monitored by K-type thermocouple. Prior to catalytic activity test, an in situ reduction of the catalyst was performed at 550 °C in 50vol.% H_2/N_2 for 2 h. Then, the mixture gas of 80 mL/min at a ratio of $H_2/CO_2/N_2$ = 4:1:3 was injected into the reactor, under a weight hourly space velocity (WHSV) of 96,000 mL/g/h, while the temperature of catalyst bed cooled down to the desired reaction temperature. After condensing and removing water by an ice bath, the effluent gas was monitored online by a GC-SP2100 gas chromatograph with a TDX-01 column and thermal conductivity (TCD) detector. In addition, a 60 h long-term stability test was performed at atmospheric pressure and 500 °C. In this experiment, the data related to CO_2 conversion, CH_4 selectivity and CH_4 yield were collected at stable state by performing the test on catalytic activity three times under each reaction condition. Catalytic performance was estimated based on the following equations:

$$CO_2\ \text{Conversion}(\%) = \frac{\left(V_{CO_2,in} - V_{CO_2,out}\right)}{V_{CO_2,in}} \times 100\% \quad (2)$$

$$CH_4\ \text{Selectivity}(\%) = \frac{V_{CH_4,out}}{\left(V_{CO_2,in} - V_{CO_2,out}\right)} \times 100\% \quad (3)$$

$$CH_4\ \text{Yield}(\%) = \frac{V_{CH_4,out}}{V_{CO_2,in}} \times 100\% \quad (4)$$

where $V_{i,\,in}$ and $V_{i,\,out}$ stand for various components (i = CO_2, CH_4) volume flow rates in and out of the reactor, respectively.

3. Results

3.1. Characterization

As shown in Figure 1a, the low-angle XRD curve of KIT-6 exhibited a sharp peak (211) at 0.97° along with a weak peak (220) at 1.10°, reflecting the structural feature of cubic Ia3d mesoporous Si [36]. Similar peaks were also detected for 10Ni-0.5V/KIT-6 and 20Ni-0.5V/KIT-6, indicating that the Ia3d mesoporous structure was retained after the introduction of Ni and V. Figure 1b displayed wide-angle XRD curve of 10Ni/KIT-6 in the range from 10° to 80°. It can be found that there was a faint peak at 44.3° matching the Ni (111) plane [37], which revealed the formation of Ni nanoparticles (2.4 nm from Table 1) due to their successful introduction inside the 3D mesopores. Similar peaks were observed for 10Ni-0.5V/KIT-6 and 20Ni-0.5V/KIT-6, suggesting that the effective confinement effect of 3D mesopores still existed after introducing the appropriate amount of Ni and V, which was beneficial for yielding small Ni nanoparticles with high dispersion, corresponding to 2.5 nm and 2.7 nm (cf. Table 1), respectively. This meant that more Ni active sites were produced to promote the catalytic performance for CO_2 methanation. Additionally, no diffraction peak of V species was observed on 10Ni-0.5V/KIT-6 or 20Ni-0.5V/KIT-6, implying that V species were well dispersed on the catalyst surface.

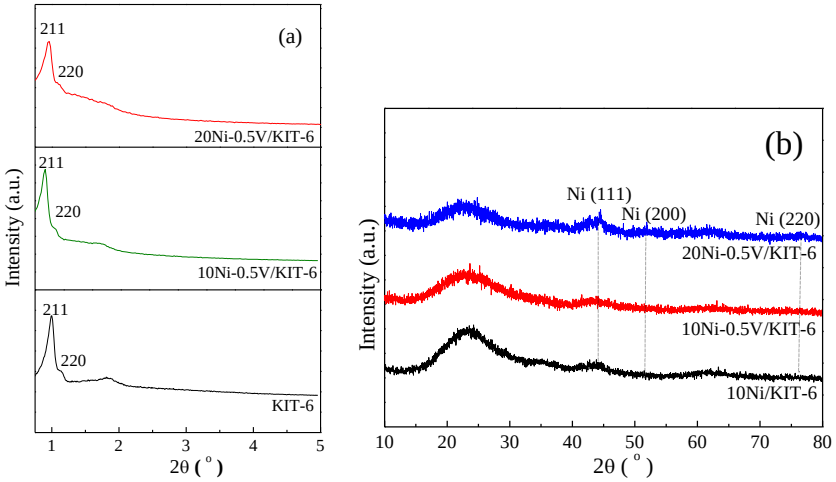

Figure 1. (**a**) Low-angle XRD patterns of support and catalysts; (**b**) Wide-angle XRD patterns of Ni-based catalysts.

Figure 2 displayed H_2-TPR profiles of Ni-based catalysts. The H_2-TPR profile of 10Ni/KIT-6 presented a successive absorption peak of H_2, for which their corresponding temperatures were 342 °C, 395 °C and 530 °C, respectively, suggesting the presence of three different NiO species [35]. The H_2-TPR curve of 10Ni-0.5V/KIT-6 slightly shifted to a higher temperature as compared to that of 10Ni/KIT-6. The low temperature peak decreased sharply, and the high temperature peak increased rapidly until it turned into the main peak, corresponding to a temperature of 535 °C. Such changes revealed that the introduction of V species boosted the metal-support interaction to enhance the reduction performance of NiO. The reduction of NiO species produced different numbers of defects in relation to interaction intensity with the support, which offered the anchoring sites for highly dispersed Ni nanoparticles. In contrast, 20Ni-0.5V/KIT-6 exhibited two distinct reduction peaks located at lower and higher temperatures with larger peak areas relative to those of 10Ni-0.5V/KIT-6 due to more

Ni loading, significantly promoting the reduction of NiO to Ni. This responded to desorption of a large number of hydrogen species in the H_2-TPD curve with H_2 uptake of 168.5 μmol/g, implying its strong ability to activate H_2. Meanwhile, as the main peak, the high temperature peak shifted to a higher temperature of 561 °C, which was very close to the reduction temperature of 550 °C, indicating that more Ni active sites could be produced, thereby improving CO_2 conversion and CH_4 selectivity. Considering the above analysis, 20Ni-0.5V/KIT-6 possessed the best reducibility of Ni and generated the most active Ni sites.

Table 1. Physicochemical properties of Ni-based catalysts.

Catalyst	Ni Particles Size (nm)	H_2 Uptake (μmol/g)	D (%) [b]	Mass Loss (%) [c]
	d_{Ni} [a]			
10Ni/KIT-6	2.4	106.0	15.8	-
10Ni-0.5V/KIT-6	2.5	157.0	23.4	-
20Ni-0.5V/KIT-6	2.7	168.5	25.1	-
spent 20Ni-0.5V/KIT-6	2.9	-	-	1.2

[a] Particles size calculated by the Debye–Scherrer equation according to Ni (111) plane. [b] Ni dispersion estimated on the basis of hydrogen temperature-programmed reduction (H_2-TPR) and hydrogen temperature-programmed desorption (H_2-TPD). [c] Mass loss was obtained by thermogravimetric analysis (TGA).

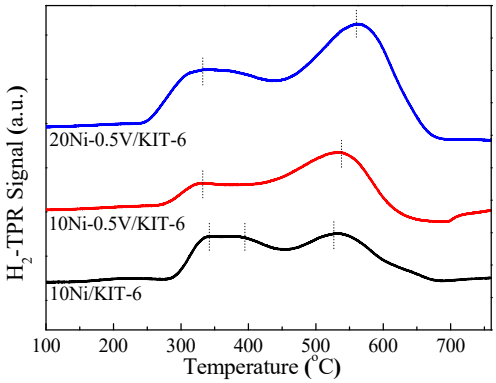

Figure 2. H_2-TPR profiles of Ni-based catalysts.

Figure 3 described the H_2-TPD profiles of 10Ni/KIT-6, 10Ni-0.5V/KIT-6 and 20Ni-0.5V/KIT-6. All profiles presented a low temperature peak below 500 °C stemming from the weak adsorption of hydrogen on defective Ni nanoparticles and a high temperature peak of about 700 °C arising from strongly adsorbed hydrogen on the subsurface of catalyst and/or spillover H_2 [35]. The low temperature peak area below 500 °C was closely related to H_2 uptake and Ni dispersion, which was considered as a key discussion, as in reference [38]. In comparison to 10Ni/KIT-6, the peak area at low temperature for 10Ni-0.5V/KIT-6 and 20Ni-0.5V/KIT-6 increased remarkably and the peak temperature shifted to higher temperature, which was ascribed to an increase in the number of Ni active sites and the high dispersion of Ni nanoparticles. Further confirmation was provided by H_2-uptakes and Ni dispersion summarized in Table 1. 10Ni-0.5V/KIT-6 exhibited better hydrogen absorption and Ni dispersion as compared to those of 10Ni/KIT-6, corresponding to H_2 uptake of 157.0 μmol/g and Ni dispersion of 23.4%, resulting from an improvement in H_2 storage due to a suitable V loading. As reported by Liu et al. [39], the H adsorbed on the Ni active site at high temperatures was transferred to low valence V species for storage, and could flow back to the Ni active site during desorption, which was responsible for high Ni dispersion. In addition, H_2 absorption capacity was directly related to Ni loading. Comparing this with 10Ni-0.5V/KIT-6, 20Ni-0.5V/KIT-6 possessed better catalytic performance owing to the incorporation of 20 wt.% NiO, which facilitated the production of more Ni active sites, suggesting that Ni nanoparticles were highly dispersed on the catalyst surface (Ni dispersion of 25.1%).

As mentioned above, the dispersion of Ni nanoparticles on 20Ni-0.5V/KIT-6 catalyst presented the best, which facilitated the conversion of the maximum amount of CO_2 to CH_4.

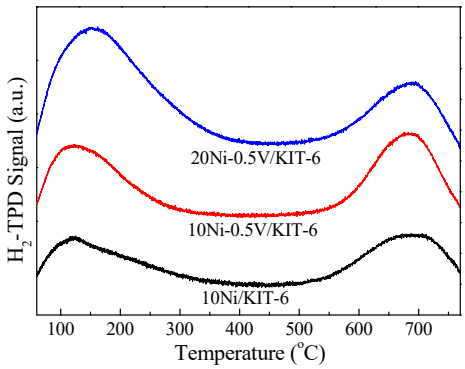

Figure 3. H_2-TPD profiles of Ni-based catalysts.

TEM images of KIT-6, 10Ni/KIT-6, 10Ni-0.5V/KIT-6 and 20Ni-0.5V/KIT-6 were illustrated in Figure 4. The 3D mesopores were regularly arranged in Figure 4a, which was indexed as (211) and (220) planes of KIT-6, respectively, according to a low-angle XRD pattern. After the introduction of Ni and V, 3D-mesoporous structure was still well preserved and no aggregation of Ni nanoparticles was observed on the outer surface of KIT-6 in Figure 4b–d. Such observations revealed that Ni nanoparticles were uniformly scattered into the internal pores, stimulating the production of small Ni nanoparticles due to the valid confinement effect of 3D mesopores and intense interaction between active Ni and KIT-6. Furthermore, dark spots on the TEM image of 20Ni-0.5V/KIT-6 stood for Ni nanoparticles, of which 50 particles were randomly chosen to estimate the particle size. The inset in Figure 4d revealed the distribution of Ni nanoparticles was mainly concentrated in 2–3 nm with an average size of around 2.8 nm, which was in line with XRD result. In Figure 4e, the EDX profile of 20Ni-0.5V/KIT-6 presented pronounced peaks involving Ni, Si, O and V species, meaning that these elements were immobilized into 3D mesopores. Therefore, abundant Ni active sites forming on the interior surface were conducive to enhancing the catalytic performance for CO_2 methanation.

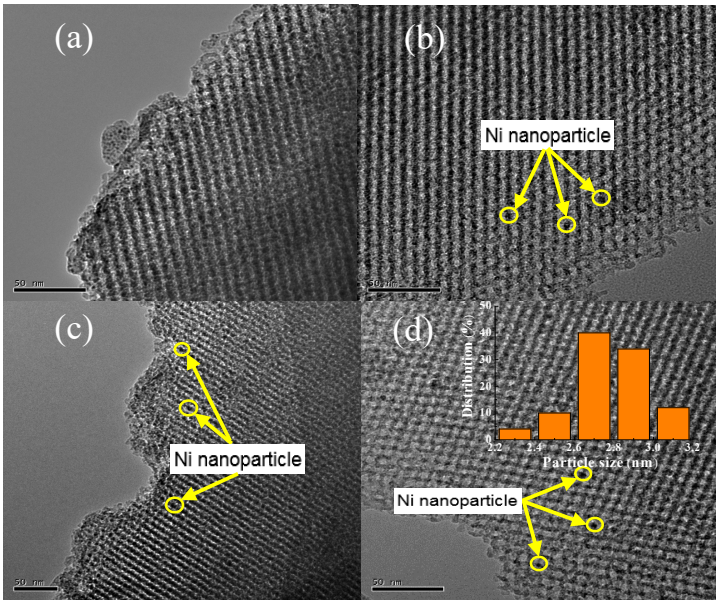

Figure 4. *Cont*.

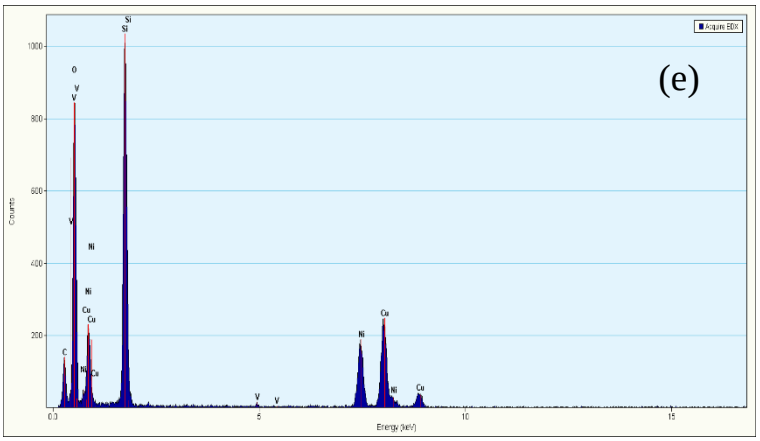

Figure 4. TEM images of (**a**) KIT-6; (**b**) 10Ni/KIT-6; (**c**) 10Ni-0.5V/KIT-6; (**d**) 20Ni-0.5V/KIT-6; (**e**) energy-dispersive X-ray spectroscopy (EDX) spectrum of 20Ni-0.5V/KIT-6.

3.2. Effect of V_2O_5 and NiO Loading

The effect of V_2O_5 loading on the catalytic performance for CO_2 methanation was described in Figure 5. Noting that, CO_2 conversion of 10Ni/KIT-6 and 10Ni-yV/KIT-6 present a volcanic curve with increasing temperature and achieved a peak value at 400 °C. This was because CO_2 methanation was an exothermic reaction and the high temperature was detrimental to the forward reaction due to the thermodynamic equilibrium limitation [17]. As a comparison of 10Ni/KIT-6, the addition of V species remarkably enhanced CO_2 conversion, and enabled the equilibrium conversion temperature to shift from 450 °C to 400 °C. Moreover, the V-containing catalyst possessed the best catalytic performance when V_2O_5 loading was 0.5 wt.%, and its catalytic performance displayed a downward trend with loadings either more or less than 0.5 wt.%, especially for 2 wt.%. It was worth noting that CO_2 conversion of 10Ni-2V/KIT-6 was only 75.4% at 400 °C, which was lower than 82.0% for 10Ni-0.5V/KIT-6. This was because excessive V species covered some of Ni active sites and subsequently lowered the ability of absorption and dissociation for CO and H_2 [35], leading to a decline in the catalytic performance. Furthermore, the CH_4 yield showed a similar trend over reaction temperature as CO_2 conversion, and 10Ni-0.5V/KIT-6 possessed CH_4 yield of 82.0% at 400 °C, which was higher than 81% of 10Ni-0.1V/KIT-6. In addition, CH_4 selectivity of 10Ni/KIT-6 reached the lowest value at 300 °C due to the formation of a large amount of CO by-products by reverse water-gas-shift (RWGS) reaction. As reported by Sun et al. [40], high temperature was detrimental to RWGS reaction. Further increasing the temperature, CH_4 selectivity of 10Ni/KIT-6 exhibited an upward trend with a subsequent decline and achieved the maximum value of 90.9% at 450 °C. The decreased CH_4 selectivity was ascribed to the occurrence of a methane steam reforming reaction, which was promoted at high temperatures [41]. In contrast, 10Ni-yV/KIT-6 held 100% CH_4 selectivity at 400 °C, which was attributed to an improved ability for CO dissociation due to the incorporation of V species [36]. Based on the above discussion, V species were able to boost the catalytic performance for CO_2 methanation, and the best catalytic performance was achieved when V_2O_5 loading was 0.5 wt.%, corresponding to 82.0% CO_2 conversion and 100% CH_4 selectivity at 400 °C.

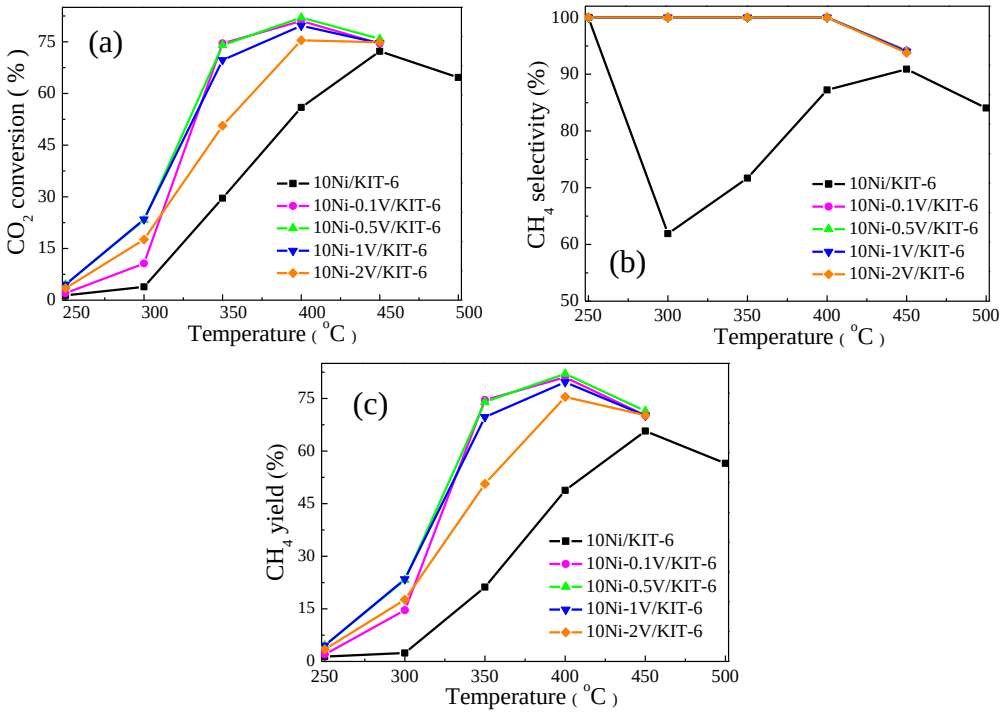

Figure 5. Catalytic performance on 10Ni/KIT-6 and 10Ni-yV/KIT-6 for CO_2 methanation: (**a**) CO_2 conversion; (**b**) CH_4 selectivity and (**c**) CH_4 yield.

Figure 6 described the effect of NiO loading on the catalytic performance for CO_2 methanation. The catalysts with various NiO loadings exhibited a similar trend in CO_2 conversion with increasing temperatures like Figure 5, and CO_2 conversion showed a decline above 350 °C due to the thermodynamic equilibrium limitation during the exothermic CO_2 methanation reaction [17]. CO_2 conversion was increasingly enhanced as NiO loading increased from 5 wt.% to 20 wt.%. Clearly, 5Ni-0.5V/KIT-6 realized its maximum CO_2 conversion of 76.3% at 425 °C, while 20Ni-0.5V/KIT-6 attained the maximum CO_2 conversion of 87.2% at merely 350 °C. However, the corresponding CO_2 conversion did not continue to elevate when NiO loading increased to 40 wt.%, implying that an appropriate amount of NiO loading could facilitate the improvement of catalytic performance. Moreover, a similar trend was observed between CH_4 yield and CO_2 conversion with increasing NiO loading and the catalyst containing 20 wt.% NiO displayed the best catalytic performance. Noting that CH_4 selectivity, for all the catalysts other than 40Ni-0.5V/KIT-6, remained almost unchanged at 100% below 425 °C and decreased at above 425 °C. Nevertheless, CH_4 selectivity of 40Ni-0.5V/KIT-6 had dropped drastically at above 400 °C. This phenomenon indicated that excess NiO caused aggregation of Ni particles to partly cover V species and subsequently reduce contact between V species and intermediate product CO, which was detrimental to CO dissociation, thus resulting in a decrease in CH_4 selectivity. To sum up, the right amount of NiO loading was conducive to the enhancement of CO_2 conversion and CH_4 selectivity. Among all the catalysts being tested, 20Ni-0.5V/KIT-6 displayed the best catalytic performance for CO_2 methanation, corresponding to 87.2% CO_2 conversion and 100% CH_4 selectivity.

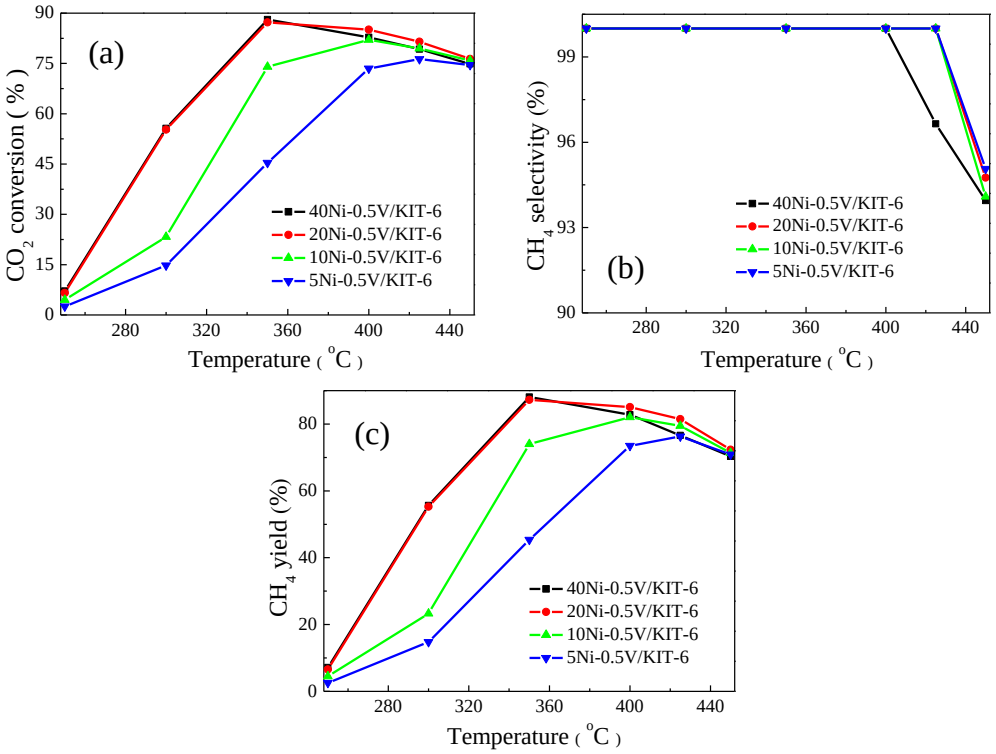

Figure 6. Catalytic performance on xNi-0.5V/KIT-6 for CO_2 methanation: (**a**) CO_2 conversion; (**b**) CH_4 selectivity and (**c**) CH_4 yield.

To further explore the relationship between the surface basicity and catalytic activity, the CO_2-TPD of 10Ni/KIT-6 and 20Ni-0.5V/KIT-6 was performed and the results were shown in Figure 7. Apparently, the CO_2-TPD profile of 10Ni/KIT-6 displayed two CO_2 desorption peaks. One was the main peak at 190 °C, which was related to medium basic sites; the other was the secondary peak at 90 °C, which was assigned to weak basic sites [42]. Compared with 10Ni/KIT-6, 20Ni-0.5V/KIT-6 presented a larger peak area with the main peak shifted to a higher temperature around 200 °C, indicative of an increase in surface basicity due to the synergistic effect from the incorporation of a correct amount of Ni and V. The strengthened surface basicity could boost the number of basic sites, which promoted CO_2 adsorption to improve catalytic performance during CO_2 methanation.

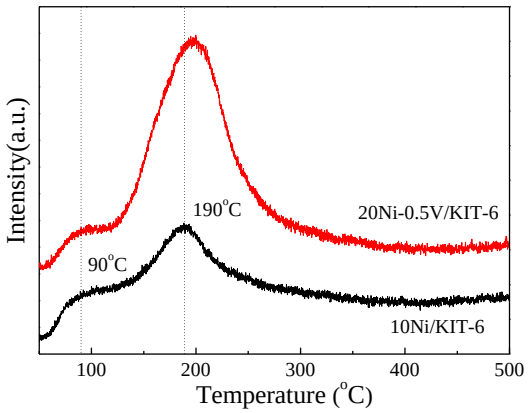

Figure 7. Carbon dioxide temperature-programmed desorption (CO_2-TPD) profiles of 10Ni/KIT-6 and 20Ni-0.5V/KIT-6.

Combined with XRD, TEM and H_2-TPD results, 20Ni-0.5V/KIT-6 possessed small-sized Ni nanoparticles with the best Ni dispersion, which was mainly responsible for the highest catalytic

activity. Additionally, the optimal reducibility of 20Ni-0.5V/KIT-6 was determined by H_2-TPR, which could produce the largest amount of Ni active sites, considerably promoting the catalytic hydrogenation of CO_2 to CH_4. Furthermore, an increased surface basicity could intensify the ability of CO_2 chemisorption, progressively enhancing the reaction with CO_2.

3.3. Stability Test of 20Ni-0.5V/KIT-6

Excellent catalytic materials for CO_2 methanation should possess both high catalytic activity at lower temperature and good catalytic stability at higher temperature. Therefore, a stability test was essential to identify superior catalytic materials. In this work, a 60 h-lifetime test on 20Ni-0.5V/KIT-6 was performed at 1atm, 500 °C and 96,000 mL/g/h, and the experimental results were illustrated in Figure 8. For 20Ni-0.5V/KIT-6, CO_2 conversion and CH_4 selectivity were constant at around 67% and 85%, respectively. Such performance was superior to those of Ni/Sr/Si catalysts, in which CO_2 conversion was less than 66% after 50 h-lifetime test at 1atm, 350 °C and 15,000 mL/g/h [43], indicating that 20Ni-0.5V/KIT-6 possessed better catalytic stability at high temperature.

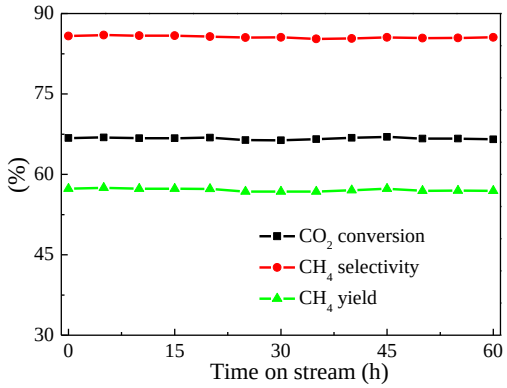

Figure 8. Catalytic stability test of 20Ni-0.5V/KIT-6.

For further analyzing the catalytic performance of 20Ni-0.5V/KIT-6, we made a comparison between our experimental results and these data reported in the literature [30,31,44–48]. As described in Table 2, several reported results with respect to various catalysts for CO_2 conversion and CH_4 selectivity at 1atm (with optimal reaction temperatures) were listed. It was apparent that 20Ni-0.5V/KIT-6 developed in this work possessed 87.2% CO_2 conversion and 100% CH_4 selectivity at 1atm, 350 °C and 96,000 mL/g/h, while it also exhibited a good stability at 500 °C for a 60 h-lifetime test, which was better than the previous reported results. Based on the above comparative analysis, 20Ni-0.5V/KIT-6, with superior catalytic activity and stability, presented a broad application prospect for CO_2 methanation.

Table 2. Comparison of CO_2 conversion and CH_4 selectivity for 20Ni-0.5V/KIT-6 in our study and some catalysts reported in the literature at 1atm with the optimum temperature.

Catalyst	Ni/NiO Content (wt.%)	T_{opt} (°C)	CO_2 Conversion (%)	CH_4 Selectivity (%)	WHSV (ml g^{-1} h^{-1})	Stability (h)	Ref.
Ni-1MgO/SiO_2	10 [a]	400	<75	<100	15,000	10	[44]
14Ni7CeUSY	14 [a]	400	68.3	95.1	-	-	[45]
15Ni/SBA-15	15	450	~70	<95	86,000	-	[30]
2Ce-20Ni/Al_2O_3	20 [a]	350	72.7	100	18,000	10	[46]
Ni-20Ce/MCM-41	20 [a]	380	85.6	99.8	9000	30	[47]
25Ni-Al_2O_3	25 [a]	350	74	99	9000	10	[48]
10Co/Al_2O_3	10 [a]	400	77.8	96.5	3600	-	[10]
0.5Ru/Na-TiO_2	0.5 [a]	450	~60	~90	90,000	-	[15]
10Ni-0.5V/KIT-6	10 [b]	400	82.0	100	96,000	-	This work
20Ni-0.5V/KIT-6	20 [b]	350	87.2	100	96,000	60	This work

[a]—Ni, Co content, [b]—NiO content.

After stability testing, spent 20Ni-0.5V/KIT-6 was characterized by TEM, TGA and XRD to further explore the sintering and carbon deposition of Ni nanoparticles on the catalyst surface. As shown in Figure 9a, spent 20Ni-0.5V/KIT-6 presented a similar TEM image as the fresh one and no aggregation of Ni nanoparticles was detected, implying that Ni nanoparticles were still highly dispersed in the 3D mesopores. From Figure 9b, spent 20Ni-0.5V/KIT-6 exhibited a similar XRD profile with a very weak diffraction peak of Ni nanoparticles at 44.3°, similar to fresh 20Ni-0.5V/KIT-6. Moreover, the average size of Ni nanoparticles estimated by the Debye–Scherrer equation was 2.9 nm, reflecting no occurrence of Ni sintering. There were two reasons for this phenomenon: firstly, the mesopore channel of the support could effectively limit Ni nanoparticles in a fixed space; secondly, strong metal support interaction blocked the migration of Ni nanoparticles on the catalytic surface during reduction and reaction at high temperatures, restricting the growth of Ni nanoparticle size. Furthermore, the carbon content deposited on spent 20Ni-0.5V/KIT-6 was assessed at only 1.2% according to TGA (cf. Table 1). Simultaneously, the XRD profile of spent 20Ni-0.5V/KIT-6 did not present the diffraction peaks of graphite carbon, and no carbon film was observed on the corresponding TEM image, suggesting an excellent anti-coking property. As identified by XRD and TEM, the sizes of Ni nanoparticles were still very small, around 3 nm after lifetime test, which could reduce the rate of carbon deposition [49]. In addition, 3D mesoporous channels also played a central role in inhibiting carbon film formation. Combining the above analysis with stability test results, 20Ni-0.5V/KIT-6 displayed excellent catalytic performance with good stability at high temperatures due to a strong metal-support interaction and effective 3D mesopores confinement effect.

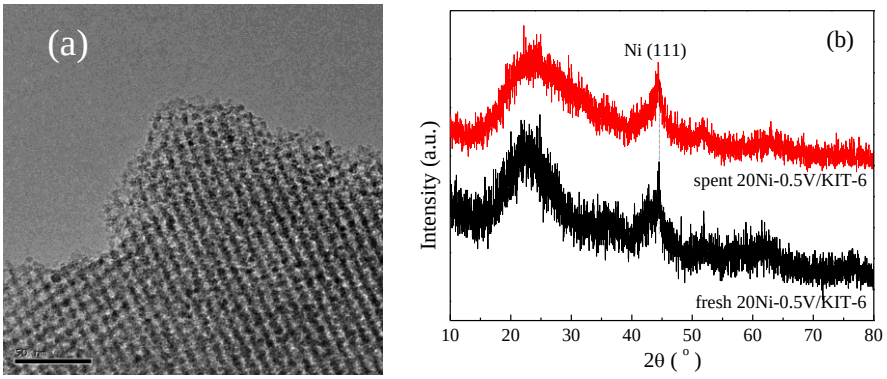

Figure 9. (**a**) TEM images of spent 20Ni-0.5V/KIT-6; (**b**) XRD profiles of fresh and spent 20Ni-0.5V/KIT-6.

4. Conclusions

In this work, several Ni-based catalysts with V species well dispersed on 3D-mesoporous KIT-6 were synthesized for the production of CH_4. Characterization results revealed that both the reducibility and dispersion of Ni were enhanced by the incorporation of V species, and further boosted with suitable amount of NiO loading. 20Ni-0.5V/KIT-6 demonstrated the best reducibility and Ni dispersion with H_2 uptake of 157.0 μmol/g and Ni dispersion of 23.4%, which facilitated producing the largest amount of Ni active sites. The synergistic effect between Ni and V could strengthen surface basicity to elevate the ability of CO_2 activity on the 20Ni-0.5V/KIT-6. Additionally, 3D mesoporous channels still remained after introducing the appropriate amount of Ni and V, which was beneficial for yielding small Ni nanoparticles. Superior catalytic performance was attained at 1 atm, 96,000 mL/g/h and a low temperature of only 350 °C, and 20Ni-0.5V/KIT-6 possessed the best catalytic performance, corresponding to 87.2% CO_2 conversion and 100% CH_4 selectivity. The exceptional catalytic performance was ascribed to the formation of well-dispersed small Ni nanoparticles, enhanced reducibility of NiO, intensified surface basicity and the effective confinement effect of 3D mesopores. Furthermore, an intimate metal-support interaction and 3D mesopores limiting effect made active Ni species tightly immobilize on the catalyst surface, resulting in a remarkably improved stability of 20Ni-0.5V/KIT-6. The catalyst with 20 wt.% NiO and 0.5 wt.% V_2O_5 presented better catalytic

stability in a 60 h-lifetime test for CO_2 methanation at 500 °C, implying promising stability under the high exothermic reaction environment. Our research indicated that the 20Ni-0.5V/KIT-6 catalyst possessed superior catalytic activity and stability and was a promising candidate for applications in CO_2 hydrogenation to methane.

Author Contributions: Conceptualization, H.C.; methodology, H.C.; software, W.W.; validation, T.C.; formal analysis, W.W.; investigation, H.C.; resources, H.W.; data curation, W.W.; writing—original draft preparation, H.C.; writing—review and editing, G.Z.; visualization, T.C.; supervision, X.R.; project administration, H.W.; funding acquisition, G.Z. All authors have read and agreed to the published version of the manuscript.

Funding: This research was funded by the Doctoral Research Startup Fund Project of Suzhou University (No. 2019jb01), College Students Innovation Training Program (No. 201810379043), Wang Hongyan Teaching Studio (No. 2016msgzs071), Innovative Research Team of Anhui Provincial Education Department (No. 2016SCXPTTD) and Key Discipline of Material Science and Engineering of Suzhou University (No. 2017XJZDXK3).

Conflicts of Interest: The authors declare no conflict of interest.

References

1. Zhang, F.F.; Guo, L.H.; Ding, Y.D.; Zhu, X.; Liao, Q. Flow pattern and CO_2 absorption in a falling film reactor with mixed aqueous solution of ionic liquid and MEA. *Appl. Therm. Eng.* **2018**, *138*, 583–590. [CrossRef]
2. Guo, C.; Duan, D.; Sun, Y.; Han, Y.; Zhao, S. Enhancing *Scenedesmus obliquus* biofilm growth and CO_2 fixation in a gas-permeable membrane photobioreactor integrated with additional rough surface. *Algal Res.* **2019**, *43*, 101620. [CrossRef]
3. Zhang, Z.E.; Cai, J.C.; Chen, F.; Li, H.; Zhang, W.X.; Qi, W.J. Progress in enhancement of CO_2 absorption by nanofluids: A mini review of mechanisms and current status. *Renew. Energy* **2018**, *118*, 527–535. [CrossRef]
4. Li, H.; Zhang, Z.E. Mining the intrinsic trends of CO_2 solubility in blended solutions. *J. CO2 Util.* **2018**, *26*, 496–502. [CrossRef]
5. Li, K.Z.; Chen, J.G. CO_2 Hydrogenation to methanol over ZrO_2-containing catalysts: Insights into ZrO_2 induced synergy. *ACS Catal.* **2019**, *9*, 7840–7861. [CrossRef]
6. Guo, C.L.; Wang, W.; Duan, D.R.; Zhao, C.Y.; Guo, F.Q. Enhanced CO_2 biofixation and protein production by microalgae biofilm attached on modified surface of nickel foam. *Bioproc. Biosyst. Eng.* **2019**, *42*, 521–528. [CrossRef] [PubMed]
7. Wang, Y.H.; Kattel, S.; Gao, W.G.; Li, K.Z.; Liu, P.; Chen, J.G.; Wang, H. Exploring the ternary interactions in Cu-ZnO-ZrO_2 catalysts for efficient CO_2 hydrogenation to methanol. *Nat. Commun.* **2019**, *10*, 1–10. [CrossRef]
8. Li, L.; Tang, D.W.; Song, Y.C.; Jiang, B.; Zhang, Q. Hydrogen production from ethanol steam reforming on Ni-Ce/MMT catalysts. *Energy* **2018**, *149*, 937–943. [CrossRef]
9. Riani, P.; Garbarino, G.; Cavattoni, T.; Canepa, F.; Busca, G. Unsupported cobalt nanoparticles as catalysts: Effect of preparation method on catalytic activity in CO_2 methanation and ethanol steam reforming. *Int. J. Hydrogen Energy* **2019**, *44*, 27319–27328. [CrossRef]
10. Li, W.H.; Ni, X.W.; Jiang, X.; Zhang, A.F.; Ding, F.S.; Liu, M.; Liu, Z.M.; Guo, X.W.; Song, C.S. ZrO_2 support imparts superior activity and stability of Co catalysts for CO_2 methanation. *Appl. Catal. B Environ.* **2018**, *220*, 397–408. [CrossRef]
11. Bailera, M.; Lisbona, P.; Romeo, L.M.; Espatolero, S. Power to gas projects review: Lab, pilot and demo plants for storing renewable energy and CO_2. *Renew. Sustain. Energy Rev.* **2017**, *69*, 292–312. [CrossRef]
12. Aziz, M.A.A.; Jalil, A.A.; Triwahyono, S.; Ahmad, A. CO_2 methanation over heterogeneous catalysts: Recent progress and future prospects. *Green Chem.* **2015**, *17*, 2647–2663. [CrossRef]
13. Arellano-Trevino, M.A.; Kanani, N.; Jeong-Potter, C.W.; Farrauto, R.J. Bimetallic catalysts for CO_2 capture and hydrogenation at simulated flue gas conditions. *Chem. Eng. J.* **2019**, *375*, 121953. [CrossRef]
14. Su, X.; Xu, J.H.; Liang, B.L.; Duan, H.M.; Hou, B.L.; Huang, Y.Q. Catalytic carbon dioxide hydrogenation to methane: A review of recent studies. *J. Nat. Gas Chem.* **2016**, *25*, 553–565. [CrossRef]
15. Petala, A.; Panagiotopoulou, P. Methanation of CO_2 over alkali-promoted Ru/TiO_2 catalysts: I. Effect of alkali additives on catalytic activity and selectivity. *Appl. Catal. B Environ.* **2018**, *224*, 919–927. [CrossRef]

16. Guo, Y.; Mei, S.; Yuan, K.; Wang, D.J.; Liu, H.C.; Yan, C.H.; Zhang, Y.W. Low-temperature CO_2 methanation over CeO_2-supported Ru single atoms, nanoclusters, and nanoparticles competitively tuned by strong metal-support interactions and H-spillover effect. *ACS Catal.* **2018**, *8*, 6203–6215. [CrossRef]
17. Liu, Q.; Wang, S.J.; Zhao, G.M.; Yang, H.Y.; Yuan, M.; An, X.X.; Zhou, H.F.; Qiao, Y.Y. CO_2 methanation over ordered mesoporous NiRu-doped CaO-Al_2O_3 nanocomposites with enhanced catalytic performance. *Int. J. Hydrogen Energy* **2018**, *43*, 239–250. [CrossRef]
18. Arandiyan, H.; Wang, Y.; Scott, J.; Mesgari, S.; Dai, H.X.; Amal, R. In situ exsolution of bimetallic Rh–Ni nanoalloys: A highly efficient catalyst for CO_2 methanation. *ACS Appl. Mater. Int.* **2018**, *10*, 16352–16357. [CrossRef]
19. Jacquemin, M.; Beuls, A.; Ruiz, P. Catalytic production of methane from CO_2 and H_2 at low temperature: Insight on the reaction mechanism. *Catal. Today* **2010**, *157*, 462–466. [CrossRef]
20. Arellano-Trevino, M.A.; He, Z.Y.; Libby, M.C.; Farrauto, R.J. Catalysts and adsorbents for CO_2 capture and conversion with dual function materials: Limitations of Ni-containing DFMs for flue gas applications. *J. CO2 Util.* **2019**, *31*, 143–1451. [CrossRef]
21. Le, T.A.; Kim, M.S.; Lee, S.H.; Kim, T.W.; Park, E.D. CO and CO_2 methanation over supported Ni catalysts. *Catal. Today* **2017**, *293–294*, 89–96. [CrossRef]
22. Ratchahat, S.; Sudoh, M.; Suzuki, Y.; Kawasaki, W.; Watanabe, R.; Fukuhara, C. Development of a powerful CO_2 methanation process using a structured Ni/CeO_2 catalyst. *J. CO2 Util.* **2018**, *24*, 210–219. [CrossRef]
23. Guo, X.P.; Peng, Z.J.; Hu, M.X.; Zuo, C.C.; Traitangwong, A.; Meeyoo, V.; Li, C.S.; Zhang, S.J. Highly active Ni-based catalyst derived from double hydroxides precursor for low temperature CO_2 methanation. *Ind. Eng. Chem. Res.* **2018**, *57*, 9102–9111. [CrossRef]
24. Bacarizaa, M.C.; Malevalb, M.; Graçac, I.; Lopesa, J.M.; Henriquesa, C. Power-to-methane over Ni/zeolites: Influence of the framework type. *Microporous Mesoporous Mat.* **2019**, *274*, 102–112. [CrossRef]
25. Le, T.A.; Kang, J.K.; Park, E.D. CO and CO_2 methanation over Ni/SiC and Ni/SiO_2 catalysts. *Top. Catal.* **2018**, *61*, 1537–1544. [CrossRef]
26. Song, F.J.; Zhong, Q.; Yu, Y.; Shi, M.G.; Wu, Y.H.; Hu, J.H.; Song, Y. Obtaining well-dispersed Ni/Al_2O_3 catalyst for CO_2 methanation with a microwave-assisted method. *Int. J. Hydrogen Energy* **2017**, *42*, 4174–4183. [CrossRef]
27. Aziz, M.A.A.; Jalil, A.A.; Triwahyono, S.; Mukti, R.R.; Taufiq-Yap, Y.H.; Sazegar, M.R. Highly active Ni-promoted mesostructured silica nanoparticles for CO_2 methanation. *Appl. Catal. B Environ.* **2014**, *147*, 359–368. [CrossRef]
28. Bacariza, M.C.; Graça, I.; Bebiano, S.S.; Lopes, J.M.; Henriques, C. Micro- and mesoporous supports for CO_2 methanation catalysts: A comparison between SBA-15, MCM-41 and USY zeolite. *Chem. Eng. Sci.* **2018**, *175*, 72–83. [CrossRef]
29. Lu, B.W.; Ju, Y.W.; Abea, T.; Kawamoto, K. Grafting Ni particles onto SBA-15, and their enhanced performance for CO_2 methanation. *RSC Adv.* **2015**, *5*, 56444–56454. [CrossRef]
30. Budi, C.S.; Wu, H.C.; Chen, C.S.; Saikia, D.; Kao, H.M. Ni nanoparticles supported on cage-type mesoporous silica for CO_2 hydrogenation with high CH_4 selectivity. *Chemsuschem* **2016**, *9*, 2326–2331. [CrossRef]
31. Lu, X.P.; Gu, F.N.; Liu, Q.; Gao, J.J.; Liu, Y.J.; Li, H.F.; Jia, L.H.; Xu, G.W.; Zhong, Z.Y.; Su, F.B. VO_x promoted Ni catalysts supported on the modified bentonite for CO and CO_2 methanation. *Fuel Process. Tech.* **2015**, *135*, 34–46. [CrossRef]
32. Li, H.D.; Ren, J.; Qin, X.; Qin, Z.F.; Lin, J.Y.; Li, Z. Ni/SBA-15 catalysts for CO methanation: Effects of V, Ce, and Zr promoters. *RSC Adv.* **2015**, *5*, 96504–96517. [CrossRef]
33. Li, B.T.; Luo, X.; Huang, J.; Wang, X.J.; Liang, Z.X. One-pot synthesis of ordered mesoporous Cu-KIT-6 and its improved catalytic behavior for the epoxidation of styrene: Effects of the pH value of the initial gel. *Chin. J. Catal.* **2017**, *38*, 518–528. [CrossRef]
34. Kleitz, F.; Choi, S.H.; Ryoo, R. Cubic Ia3d large mesoporous silica: Synthesis and replication to platinum nanowires, carbon nanorods and carbon nanotubes. *Chem. Commun.* **2003**, *17*, 2136–2137. [CrossRef] [PubMed]
35. Cao, H.X.; Zhang, J.; Guo, C.L.; Chen, J.G.; Ren, X.K. Highly dispersed Ni nanoparticles on 3D-mesoporous KIT-6 for CO methanation: Effect of promoter species on catalytic performance. *Chin. J. Catal.* **2017**, *38*, 1127–1137. [CrossRef]

36. Cao, H.X.; Zhang, J.; Guo, C.L.; Chen, J.G.; Ren, X.K. Modifying surface properties of KIT-6 zeolite with Ni and V for enhancing catalytic CO methanation. *Appl. Surf. Sci.* **2017**, *426*, 40–49. [CrossRef]
37. Cao, H.X.; Zhang, J.; Ren, X.K.; Guo, C.L. Enhanced CO methanation over Ni-based catalyst using a support with 3D-mesopores. *Korean J. Chem. Eng.* **2017**, *34*, 2374–2382. [CrossRef]
38. Velu, S.; Gangwal, S.K. Synthesis of alumina supported nickel nanoparticle catalysts and evaluation of nickel metal dispersions by temperature programmed desorption. *Solid State Ion.* **2006**, *177*, 803–811. [CrossRef]
39. Liu, Q.; Gu, F.N.; Lu, X.P.; Liu, Y.J.; Li, H.F.; Zhong, Z.Y.; Xu, G.W.; Su, F.B. Enhanced catalytic performances of Ni/Al_2O_3 catalyst via addition of V_2O_3 for CO methanation. *Appl. Catal. A* **2014**, *488*, 37–47. [CrossRef]
40. Sun, F.M.; Yan, C.F.; Wang, Z.D.; Guo, C.Q.; Huang, S.L. Ni/Ce–Zr–O catalyst for high CO_2 conversion during reverse water gas shift reaction (RWGS). *Int. J. Hydrogen Energy* **2015**, *40*, 15985–15993. [CrossRef]
41. Ding, M.Y.; Tu, J.L.; Zhang, Q.; Wang, M.L.; Tsubaki, N.; Wang, T.J.; Ma, L.L. Enhancement of methanation of bio-syngas over CeO_2-modified Ni/Al_2O_3 catalysts. *Biomass Bioenergy* **2016**, *85*, 12–17. [CrossRef]
42. Quindimil, A.; De-La-Torre, U.; Pereda-Ayo, B.; González-Marcos, J.A.; González-Velasco, J.R. Ni catalysts with La as promoter supported over Y- and BETA- zeolites for CO_2 methanation. *Appl. Catal. B-Environ.* **2018**, *238*, 393–403. [CrossRef]
43. Guo, M.; Lu, G.X. The difference of roles of alkaline-earth metal oxides on silica-supported nickel catalysts for CO_2 methanation. *RSC Adv.* **2014**, *4*, 58171–58177. [CrossRef]
44. Guo, M.; Lu, G.X. The effect of impregnation strategy on structural characters and CO_2 methanation properties over MgO modified Ni/SiO_2 catalysts. *Catal. Commun.* **2014**, *54*, 55–60. [CrossRef]
45. Graça, I.; González, L.V.; Bacariza, M.C.; Fernandes, A.; Henriques, C.; Lopes, J.M.; Ribeiro, M.F. CO_2 hydrogenation into CH_4 on NiHNaUSY zeolites. *Appl. Catal. B* **2014**, *147*, 101–110. [CrossRef]
46. Rahmani, S.; Rezaei, M.; Meshkani, F. Preparation of promoted nickel catalysts supported on mesoporous nanocrystalline gamma alumina for carbon dioxide methanation reaction. *J. Ind. Eng. Chem.* **2014**, *20*, 4176–4182. [CrossRef]
47. Wang, X.L.; Zhu, L.J.; Liu, Y.C.; Wang, S.R. CO_2 methanation on the catalyst of Ni/MCM-41 promoted with CeO_2. *Sci. Total. Environ.* **2018**, *625*, 686–695. [CrossRef]
48. Daroughegi, R.; Meshkani, F.; Rezaei, M. Enhanced activity of CO_2 methanation over mesoporous nanocrystalline $Ni-Al_2O_3$ catalysts prepared by ultrasound-assisted co-precipitation method. *Int. J. Hydrogen Energy* **2017**, *42*, 15115–15125. [CrossRef]
49. Liu, Q.; Gao, J.J.; Gu, F.N.; Lu, X.P.; Liu, Y.J.; Li, H.F.; Zhong, Z.Y.; Liu, B.; Xu, G.W.; Su, F.B. One-pot synthesis of ordered mesoporous Ni–V–Al catalysts for CO methanation. *J. Catal.* **2015**, *326*, 127–138. [CrossRef]